The role of ocean cooling in setting glacial southern source bottom water salinity

M. D. Miller,[1] J. F. Adkins,[2] D. Menemenlis,[3] and M. P. Schodlok[3,4]

Received 23 February 2012; revised 2 May 2012; accepted 20 June 2012; published 4 August 2012.

[1] At the Last Glacial Maximum (LGM), the salinity contrast between northern source deep water and southern source bottom water was reversed with respect to the contrast today. Additionally, Glacial Southern Source Bottom Water (GSSBW) was saltier than Antarctic Bottom Water (AABW), over and above the difference implied by the mean sea level change. This study examines to what extent cold temperatures, through their effect on ice formation and melting, could have caused these differences. Computational sensitivity experiments using a coupled ice shelf cavity–sea ice–ocean model are performed in a Weddell Sea domain, as a representative case study for bottom water formation originating from Antarctic continental shelves. Ocean temperatures at the domain open boundaries are systematically lowered to determine the sensitivity of Weddell Sea water mass properties to a range of cool ocean temperatures. The steady state salinities differ between experiments due to temperature-induced responses of ice shelf and sea ice melting and freezing, evaporation and open boundary fluxes. The results of the experiments indicate that reduced ocean temperature can explain up to 30% of the salinity difference between GSSBW and AABW, primarily due to decreased ice shelf melting. The smallest and most exposed ice shelves, which abut narrow continental shelves, have the greatest sensitivity to the ocean temperature changes, suggesting that at the LGM there could have been a shift in geographical site dominance in bottom water formation. More sea ice is formed and exported in the cold ocean experiments, but the effect of this on salinity is negated by an equal magnitude reduction in evaporation.

Citation: Miller, M. D., J. F. Adkins, D. Menemenlis, and M. P. Schodlok (2012), The role of ocean cooling in setting glacial southern source bottom water salinity, *Paleoceanography*, *27*, PA3207, doi:10.1029/2012PA002297.

1. Introduction

[2] Paleo reconstructions of deep ocean salinity and temperature at the Last Glacial Maximum (LGM; see Table 1 for abbreviations) indicate that ocean density gradients were primarily set by salinity. Recent modeling studies [*Bouttes et al.*, 2009, 2010] suggest that this stratification could have had a significant impact on the rate of the mean overturning circulation and the carbon cycle, but it is unknown whether or by what mechanism the salinity/density gradient could have been created and maintained. We investigate to what extent sea ice–ice sheet–ocean interactions over the Antarctic continental shelves could explain this change in salinity structure.

[3] At the LGM the sea level was around 125 m lower than it is today due to the expansion of continental ice sheets, corresponding to an average ocean salinity increase of roughly 1.2 g kg^{-1}. The salinity of Atlantic Glacial Southern Source Bottom Water (GSSBW) at the LGM was 2.3 g kg^{-1} higher than that of modern Antarctic Bottom Water (AABW), leaving 1.1 g kg^{-1} unexplained by a contraction of the oceans [*Adkins et al.*, 2002]. Water at sites occupied by northern source intermediate/deep water at the LGM was saltier as well, but the salinity increase there roughly matched the average, or was slightly lower. Thus at the LGM the Atlantic Ocean deep water masses were more stratified in salinity. As $\delta^{18}O$ measurements show that deep ocean temperatures were all similar and close to the freezing point [*Adkins et al.*, 2002; *Malone et al.*, 2004; *Schrag et al.*, 2002], density gradients would have been primarily set by salinity. The observed glacial salinity stratification, when compared to the modern temperature stratification, corresponds to a higher than modern density stratification between northern and southern deep water. In addition, the LGM version of NADW, Glacial North Atlantic Intermediate Water (GNAIW), was fresher than GSSBW in the

[1]Mechanical Engineering, California Institute of Technology, Pasadena, California, USA.
[2]Geological and Planetary Sciences, California Institute of Technology, Pasadena, California, USA.
[3]Jet Propulsion Laboratory, California Institute of Technology, Pasadena, California, USA.
[4]Joint Institute for Regional Earth System Science and Engineering, University of California, Los Angeles, California, USA.

Corresponding author: M. D. Miller, Mechanical Engineering, California Institute of Technology, MC 131-24, 1200 E. California Blvd., Pasadena, CA 91125, USA. (madeline@caltech.edu)

0883-8305/12/2012PA002297

Table 1. Abbreviations Used in Text

Abbreviation	Full Name	Description
AABW	Antarctic Bottom Water	bottom water originating from Antarctica, traceable to 40°N
ACC	Antarctic Circumpolar Current	ocean current system that circumnavigates the Antarctic Continent
ASW	Antarctic Surface Water	surface water around Antarctica that interacts directly with the atmosphere
CDW	Circumpolar Deep Water	intermediate water mass of ACC
ESW	Eastern Shelf Water	product of CDW and meltwater from the eastern Weddell ice shelves
FRIS	Filchner-Ronne Ice Shelf	largest ice shelf in Weddell Sea, largest ice shelf (by volume) in Antarctica
GNAIW	Glacial North Atlantic Intermediate Water	northern source intermediate water that existed during the LGM - corresponds roughly to modern NADW, but existed at shallower depths with modified properties
GSSBW	Glacial Southern Source Bottom Water	southern source bottom water that existed during the LGM
HSSW	High Salinity Shelf Water	water formed on continental shelves of Antarctica through sea ice formation, $S > 34.5$
ISW	Ice Shelf Water	water formed in sub-ice shelf cavities - defined as water with potential temperature lower than the surface freezing point ($\lesssim -1.9°C$)
LGM	Last Glacial Maximum	time period corresponding to most recent relative maximum of continental ice sheet size, ≈20,000 years before present
MWDW	Modified Warm Deep Water	transition water mass between WW and WDW, likely source of continental shelf water masses
NADW	North Atlantic Deep Water	water mass that originates from North Atlantic, identifiable in global ocean data sets as a deep salinity maximum
WDW	Warm Deep Water	modified form of CDW found in Weddell Sea identified by temperature and salinity maximum around 300–600 m
WSDW	Weddell Sea Deep Water	water in Weddell Sea that lies above WSBW and outflows to become AABW
WSBW	Weddell Sea Bottom Water	deepest water mass in Weddell Sea, densest and coldest water mass around Antarctica, contributes eventually to AABW after mixing upward to become WSDW
WW	Winter Water	water mass defining winter mixed layer of Weddell Sea, formed from underlying WDW and brine rejection

Atlantic, which is opposite in sign to the salinity difference between NADW and AABW today.

[4] In the modern, NADW is a precursor to AABW. AABW has a lower salinity than NADW due to modifications that occur in the Southern Ocean. The properties of NADW help determine these Southern Ocean processes and how they contribute to the final characteristics of AABW. The salinity maximum that distinguishes NADW from other water masses identifies it as the main contributor to Circumpolar Deep Water (CDW) [*Reid and Lynn*, 1971]. CDW interacts with water masses formed and modified over the Antarctic continental shelves to eventually transform into AABW. In the Southern Ocean there is an excess of precipitation over evaporation, and over the Antarctic continental shelves there is an additional freshwater input from basal melting of marine-based ice sheets inside ice shelf cavities. Brine rejection from sea ice combined with sea ice export compensates for these freshwater fluxes over continental shelves, such that the salinity of continental shelf waters can be as high or higher than that of CDW. Antarctic continental shelf water properties, in particular those in the Weddell and Ross Seas and on the Adélie Coast, determine the properties of AABW. The details of how continental shelf waters are transformed to AABW and the properties of AABW vary with location, but they share many general similarities. There is also evidence that water exported from the Weddell Sea makes up more than half of AABW [*Orsi et al.*, 1999]. Therefore we consider the modern Weddell Sea as a representative source of AABW formation in our study.

[5] A detailed review of the modern processes responsible for water masses in the Weddell Sea and how they contribute to bottom water formation can be found in *Nicholls et al.* [2009] and references therein. Figure 1 shows the Θ_0/S properties of water masses on the modern Weddell Sea continental shelf. A subset of these water masses can be used to illustrate the main processes that contribute to AABW properties. Brine rejection and sea ice export in the Weddell Sea form High Salinity Shelf Water (HSSW: $S > 34.5$), the highest density water formed on the continental shelf. Ice Shelf Water (ISW: $\Theta_0 < -1.9°C$), the second highest density continental shelf water mass, is formed in large part from ice shelf meltwater. Overflows of ISW and HSSW entrain other water along their paths to the abyssal Weddell Sea, primarily diluted CDW in the form of Warm Deep Water and Modified Warm Deep Water (MWDW). The original properties of ISW, HSSW and modified CDW are evident in Weddell Sea Bottom Water (WSBW) and Weddell Sea Deep Water (WSDW), the deepest Weddell Sea water masses. The export of WSDW at the northwest boundary of the Weddell Sea is the Weddell Sea's main contribution to AABW [*Fahrbach et al.*, 1995; *Foldvik et al.*, 2004; *Gordon et al.*, 2010]. Sea ice and ice shelves, by determining the properties of ISW and HSSW, heavily influence the final properties of AABW.

[6] In the balance of these processes, AABW is fresher than NADW, but the salinity difference between the two is slight (∼0.1 g/kg) [*Nicholls et al.*, 2009; *Orsi et al.*, 1999; *Toggweiler and Samuels*, 1995]. While salinity plays a role in the local sinking of Antarctic continental shelf waters, the density difference between the two water masses is dominated by temperature; AABW is denser than NADW because it is colder.

[7] Why was the LGM deep Atlantic Ocean so salty and why did the contrast in salinity between northern source and southern source deep waters switch? In addition to having an increased ice volume, the glacial Antarctic ice sheet was

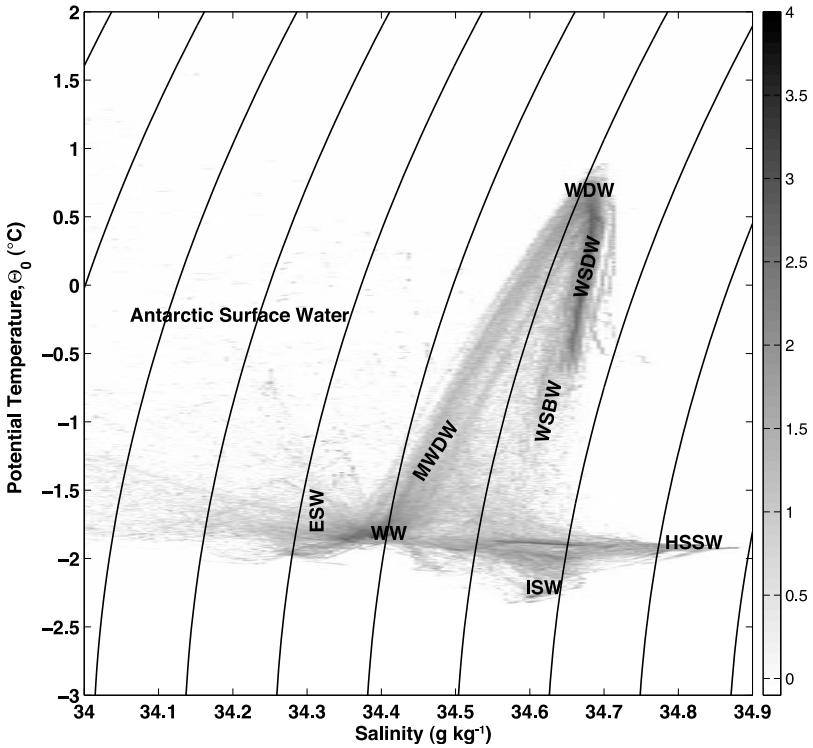

Figure 1. Histogram of modern Weddell Sea continental shelf properties (figure after *Nicholls et al.* [2009]). See Table 1 for water mass abbreviations. Continental shelf in this figure is defined after *Nicholls et al.* [2009] as south of 70°S and west of 0°. Curved lines are surface isopycnals separated by 0.1 kg m^{-3}. Gray scale shows the base 10 logarithm of the frequency of each value. Bin sizes are 0.005 in both S and Θ_0.

characterized by a northward-shifted grounding line [*Hall*, 2009; *Whitehouse et al.*, 2012]. Further, it is likely that the wind-forcing of the Southern Ocean at the LGM differed from its present state [*Toggweiler et al.*, 2006]. Undoubtedly these features had a significant role in setting glacial ocean circulation. However, long before the ice sheets expanded to their most recent maximum extent, the mean deep ocean temperature had already cooled ~1.5–2°C below its temperature during the last interglacial and during the modern periods [*Chappell and Shackleton*, 1986; *Cutler et al.*, 2003]. The approach to the LGM ocean and ice sheet states may have been initiated by this advance cooling and its resultant feedbacks.

[8] In this study, we hypothesize that the cool ocean temperatures prior to and during the LGM can account for a significant portion of the increased southern source bottom water salinity observed at the LGM, due to a reduction in freshwater from ice shelf basal melting and an increase in salinity from sea ice processes on the Antarctic continental shelves. To test this hypothesis, we perform a set of numerical ocean cooling sensitivity experiments in a regional Weddell Sea domain. We examine how ocean properties on the continental shelf change in response to lower ocean temperatures and changes in ice - ocean interactions in the Weddell Sea. We additionally consider the relative influence of ice shelves versus sea ice in setting continental shelf water properties, and how the balance between the two changes in response to increasingly cool temperatures.

[9] As modern bottom water formation depends on the complex interaction between sea ice, ice shelves and the ocean, our experiments use an ocean general circulation model (ocean GCM) coupled to dynamic/thermodynamic sea ice and thermodynamic ice shelf cavity models. While the ice sheet's total contribution to the freshwater and thermodynamic budgets plays a key role in setting modern deep water formation, the distributed locations of meltwater injection and their interactions with ocean and sea ice dynamics cannot be neglected [*Hellmer*, 2004]. Further, due to the complex interactions of different components of the ice-ocean-atmosphere system, it is difficult to predict how the system will respond to a temperature change. For example, observed Antarctic sea ice area has not decreased in response to warming ocean temperatures [*Zwally et al.*, 2002].

2. Methods

2.1. Model Setup

[10] We use the Massachusetts Institute of Technology general circulation model (MITgcm) [*Marshall et al.*, 1997a, 1997b] in a regional domain configuration to investigate the effect of ocean cooling on ice shelf and sea ice processes. The integration domain (Figure 2) is derived from a global cube sphere grid configuration with horizontal grid spacing of ~18 km [*Menemenlis et al.*, 2008]. It encompasses the Weddell Sea and the ocean bordering Queen Maud Land, and it extends slightly into the Antarctic Circumpolar

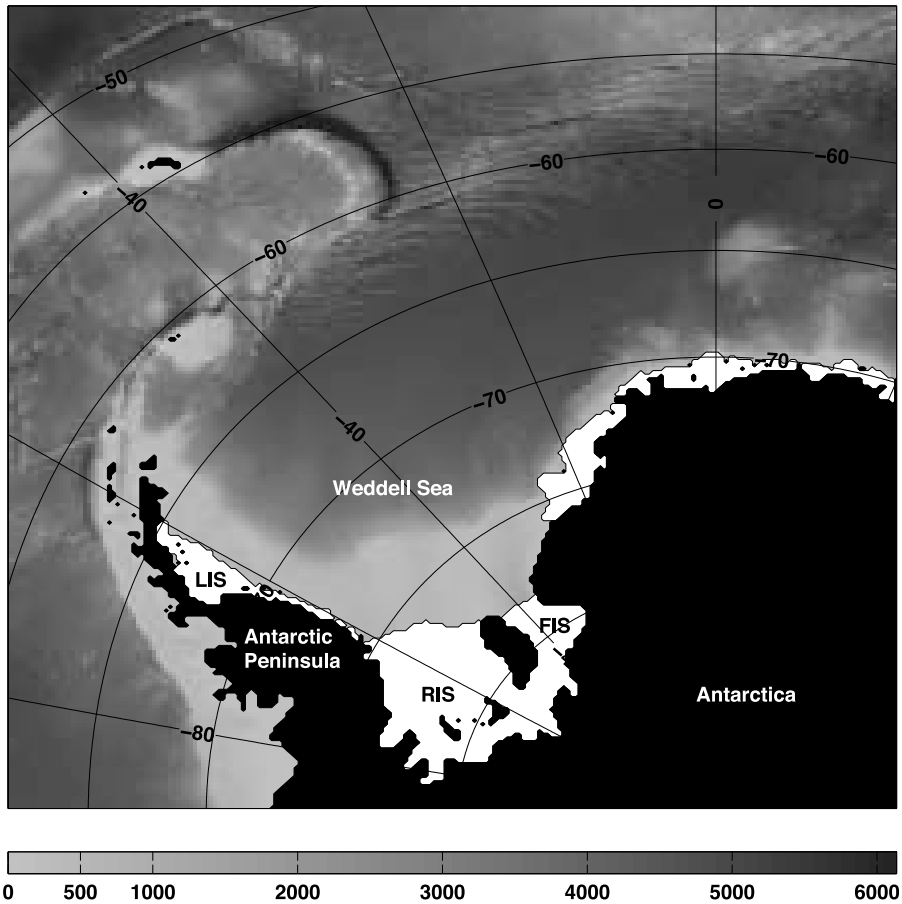

Figure 2. Computational domain and bathymetry. White area indicates floating ice shelves and black area is land/grounded ice comprising the Antarctic continent. LIS: Larsen Ice Shelf, RIS: Ronne Ice Shelf, FIS: Filchner Ice Shelf. We do not include ice shelves west of the Antarctic Peninsula. Model domain bathymetry in meters is represented by the gray scale. In the following analyses we use the space between the ice shelf front and the 1000-m contour as the continental shelf in order to include water in the Filchner and Ronne depressions in our analysis. Note that water under the ice shelves is not included, except when specified, but the water found equatorward of the eastern Weddell ice shelves is included.

Current (identified in the model by surface velocities greater than 0.5 m/s). It also covers a small section of the Bellinghausen Sea west of the Antarctic Peninsula. Ocean bathymetry is from the so-called S2004 blend [*Marks and Smith*, 2006]. Ice shelf cavity bathymetry for the Filchner-Ronne Ice Shelf (FRIS) and for the Larsen Ice Shelf in the Weddell Sea as well as for the Eastern Ice Shelves are derived from BEDMAP [*Lythe et al.*, 2001], and ice shelf thicknesses are taken from *DiMarzio et al.* [2007] using firn corrections from *van den Broeke et al.* [2008].

[11] The MITgcm is a three-dimensional general circulation model, which solves the primitive equations for fluid on a rotating sphere. Our MITgcm configuration uses the hydrostatic and Boussinesq approximations. The effect of turbulent eddy transport and mixing are parameterized by a combination of several schemes. There is a diffusive flux of properties along isoneutral surfaces proportional to the local gradient of the properties as described in *Redi* [1979]. The advective component of turbulence is approximated using the *Griffies* [1998] skew flux formulation of the *Gent and McWilliams* [1990] eddy transport velocity. To account for vertical mixing due to boundary layer dynamics and to unresolved processes such as shear instabilities, internal wave activity, and convection, we include the K-Profile Parameterization (KPP) scheme [*Large et al.*, 1994]. Using the Gent-McWilliams/Redi parameterization in combination with the KPP requires an additional flux/slope tapering scheme to remove spurious interactions between the parameterizations [*Large et al.*, 1997]. The physical equations are integrated using a finite volume discretization in locally orthogonal curvilinear coordinates, with the vertical dimension described by level coordinates. There are 50 vertical levels with thicknesses that increase monotonically from 10 m near the surface to 456 m at the deepest level. The bathymetry is represented using the partial cell formulation of *Adcroft et al.* [1997] with a minimum fraction equal to 0.3.

[12] The ocean model is coupled to the dynamic and thermodynamic sea ice model described in *Losch et al.* [2010]. Our configuration assumes that the sea ice has no heat capacity, a setup commonly described as a "zero-layer model" of the thermodynamics. Sea ice model parameters are adjusted using a Green's function approach [*Menemenlis et al.*, 2005]. Data constraints include sea ice thickness from

Upward Looking Sonar (ULS) [*Harms et al.*, 2001] and ice motion from satellite passive microwave data [*Kwok et al.*, 1998]. Optimized parameters include ocean albedo (0.15), dry ice albedo (0.88), wet ice albedo (0.79), dry snow albedo (0.95), wet snow albedo (0.82), air/ocean drag (1.02), air/ice drag (0.0012), ocean/ice drag (0.0055), ice strength P^* (12500 N m^{-2}), and lead closing H_o (1.0). See *Nguyen et al.* [2011] for a detailed description of the above parameters and of the optimization methodology.

[13] The thermodynamic ice shelf cavity model is that described in *Losch* [2008]. The shape and thickness of the ice shelves do not change as a result of melting or freezing at the interface, but there is a time-dependent flux of heat and freshwater between the ice shelf and the ocean. The fundamental melt-freeze process is defined by "three-equation thermodynamics" [*Hellmer and Olbers*, 1989; *Jenkins et al.*, 2001].

[14] Exchange of heat and freshwater between the base of the ice sheet and the ocean is parameterized as a diffusive turbulent tracer flux of temperature or salinity. Following *Holland and Jenkins* [1999], turbulent diffusivities of temperature and salinity are, respectively, $\gamma_T = 10^{-4}$ m s^{-1} and $\gamma_S = 5.05 \times 10^{-7}$ m s^{-1}. Freshwater flux in kg m^{-2} s^{-1} is

$$q = \frac{\rho c_p \gamma_T}{L}(T_b - T) + \frac{\rho_I c_{p,I} \kappa}{Lh}(T_b - T_s), \quad (1)$$

where positive q values indicate melting, ρ is the density of seawater determined by the nonlinear equation of state of *Jackett et al.* [2006], ρ_I is the density of ice (917 kg m^{-3}), c_p is the specific heat of seawater (3974 J kg^{-1} K^{-1}), $c_{p,I}$ is that of ice (2000 J kg^{-1} K^{-1}), L is the latent heat of fusion (334 kJ kg^{-1}), κ is the conductivity of heat through the ice (1.54×10^{-6} m^2 s^{-1}), and h is the local thickness of the ice shelf, which varies in space but is constant in time. T is in situ ocean temperature in °C, computed as a volume-weighted average of the two levels of ocean below the ice shelf grid cells, T_b is the temperature at the ice interface, which is assumed to be at the in situ freezing point, and T_s denotes the surface temperature of the ice shelf, here a constant −20°C. While the water freezing point in the ocean model is calculated from the non-linear equation of state of *Jackett et al.* [2006], the in situ freezing point in the ice shelf equations is determined from the linearized equation of state:

$$T_b = 0.0901 - 0.0575\, S_b - 7.61 \times 10^{-4}\, p_b, \quad (2)$$

where S_b is the salinity and p_b is the in situ pressure in dBar of the water at the ice interface. Pressure is computed using the hydrostatic approximation. The salt flux at the interface is a virtual salinity flux calculated from:

$$q(S_b - S_I) = \rho\, \gamma_s (S_b - S), \quad (3)$$

where S is ocean salinity computed in the same water volume as T. S_I is the ice salinity, which we take to be 0. The above three equations are solved for S_b, T_b, and q. The contribution to the ocean is then given by an advective tracer flux to the ocean:

$$\rho K \frac{\partial X}{\partial z} = (\rho\, \gamma_X - q)(X_b - X), \quad (4)$$

where X is the tracer, either T or S, and K is the vertical eddy diffusivity of the mixing scheme (M. Losch, personal communication, 2010).

2.2. Salinity Tracers

[15] In order to distinguish salinity changes originating from ice shelf basal melt or freeze from those occurring at the surface ocean interface with sea ice and the atmosphere, we augment our copy of the MITgcm code with two new three-dimensional tracers. One tracer tracks changes in grid cell salinity from the ice shelf, while the other accumulates salinity changes resulting from surface processes. In our model configuration, the ice shelf and sea ice freshwater fluxes, in addition to salt rejected from sea ice, are applied to the surface level of the salinity field as virtual salinity fluxes, that is, the freshwater flux is converted to an equivalent salinity flux and does not change the volume of the grid cell to which it is added. Each tracer adds the values of its respective virtual salinity fluxes to the top layer of a three-dimensional passive tracer field at each time step, which then evolve in time and space in the same manner as the salt field. We do not separate surface salt fluxes due to precipitation, evaporation, and runoff from those due to freezing and melting of sea ice in our surface salt tracer for reasons discussed later in the text.

2.3. Boundary Conditions

[16] The same year (1994) of lateral and surface boundary conditions is repeated for every year of the 50-year control and sensitivity integrations in order to force the model to a quasi-steady state, which is reached after about 30 model years. We consider steady state to be the period in the integration after which the variations in yearly-mean change of the domain-averaged salinity and temperature values are, respectively, less than 10^{-4}% and 10^{-2}%, which corresponds to approximately 2×10^{-5} g kg^{-1} and 10^{-3} °C. Values we report as steady state are averages over the final 10 years of each integration.

[17] Lateral and surface boundary conditions for the control experiment are taken from year 1994 of an Estimating the Circulation and Climate of the Ocean, Phase 2 (ECCO2) solution known as "cube78". The cube78 solution was obtained using model Green's functions to adjust a global, eddying ocean and sea ice configuration of the MITgcm [*Menemenlis et al.*, 2008]. The prescribed lateral boundary conditions are temperature, salinity, velocity of water and sea ice, sea ice area, and sea ice thickness. Oceanic boundary conditions are prescribed as monthly-mean values, which are interpolated in time to each model time step (1200 s) in order to avoid temporal discontinuities. Sea ice boundary conditions are interpolated to the model time step from daily-mean values.

[18] Surface boundary conditions (six-hourly downwelling short wave and long wave radiation, 10-meter wind velocity, 2-meter atmospheric temperature and humidity, and precipitation) used for the cube78 solution are primarily based on the European Centre for Medium-Range Weather Forecasts (ECMWF) 40-year reanalysis (ERA-40) [*Uppala et al.*, 2005] except for precipitation, which is primarily based on the Global Precipitation Climatology Project (GPCP) [*Adler et al.*, 2003]. Surface atmospheric conditions remain the

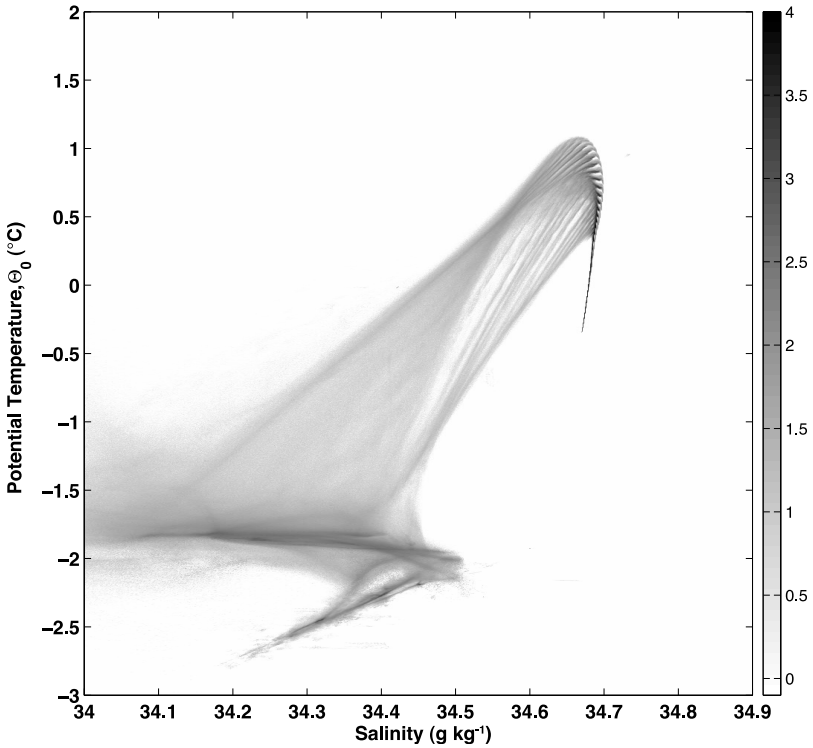

Figure 3. Histogram of control integration continental shelf properties. Weddell Sea continental shelf is defined after *Nicholls et al.* [2009] to be south of 70°S and west of 0°. Gray scale shows the base 10 logarithm of the frequency of each value. Bin sizes are 0.001 in both S and Θ_0.

same throughout all the experiments; they are all forced with the cube78 surface atmospheric conditions. However, because heat and water fluxes at the surface are diagnosed, they are able to vary with changing surface ocean temperature. Specifically, surface heat flux and evaporation are calculated using the *Large and Pond* [1982] bulk formulae, and surface wind stress is calculated using the drag coefficient parameterization of *Large and Yeager* [2004].

[19] All control and sensitivity experiments are initialized from rest and from temperature and salinity values from the January World Ocean Atlas 2009 (WOA09) [*Locarnini et al.*, 2010; *Antonov et al.*, 2010] interpolated onto our model grid. Data used to construct WOA09 are sparse in this region, particularly inside the ice shelf cavities, as ocean and ice conditions limit observations.

2.4. Control Integration Comparison With Data

[20] Our control integration generally resembles modern data in the Weddell Sea, despite some significant deficiencies. We note that the modern data shown here are distinct from those used as our initial condition. Figures 1 and 3 are logarithmic (base 10) histograms of modern data and control experiment properties over the continental shelf. They are plotted as histograms in order to highlight the water masses that are most typical, but the scales are not comparable between figures.

[21] Modern data sampling occurs during Southern Hemisphere summer; therefore the plot of our control experiment shows points from October to June. Seasonal transitions in our control may not correspond exactly to seasonal transitions in the modern, so our control experiment might have more winter type water properties than the modern data. Taking measurements near or under ice shelves is difficult, which is another source of differences between the model results and the data. In our computational setup we can easily sample at every point below the ice shelves. This is why our control ISW potential temperatures have values as low as −3°C, which corresponds to the in situ freezing point at the deepest points of the ice shelf base. HSSW in our integration is very low in salinity with respect to modern values; maximum values are 34.5 g kg^{-1} as opposed to the observed 34.9 g kg^{-1}. One likely reason for this is that sub-grid-scale sea ice processes are parameterized, and a faithful representation of their effect on salinity depends on parameter optimization. Sea ice behaves differently in the presence of ice shelves such that the model parameters must be re-optimized in their presence. However, even if the sea ice parameters were perfectly optimized to reproduce modern continental shelf properties, there would be no guarantee that these parameters would give a realistic solution under glacial conditions.

[22] Our control experiment's representation of WDW is slightly warmer than that observed. WDW is a diluted version of CDW, so it is possible that our control experiment's version is simply less diluted in temperature. Additionally over the computational continental shelf we find more points with properties of modern Antarctic Surface Water than apparent in the data, which typically is characteristic of the open ocean away from the continental shelf. This could be because the Weddell Gyre intrudes farther onto the shelf in

the model than observed, probably as a result of the grid discretization.

[23] The control integration's representation of WSDW and WSBW is very narrow in property space and essentially determined by the boundary conditions. The absence of HSSW explains in part the absence of typical WSDW and WSBW, as HSSW mixes with WDW to form these two. Still, it is not necessary that HSSW take on its most extreme value in salinity to form deep water; in fact both WDW and WSDW are higher in salinity than WSBW but have lower densities than WSBW due to their warmer temperatures.

[24] Although the control experiment produces low salinity HSSW, there is another reason why we observe a gap in property space between the control HSSW and WDW. The rapid increase of vertical grid size close to the depth of the shelf break, in combination with the coarse horizontal resolution, cause shelf properties to mix away rapidly. As a result, there is negligible transport from the shelf to the deep ocean in our experiments. Resolution of dense overflows in the modern Weddell Sea requires Δ z and Δ h < 100 m [*Legg et al.*, 2006; *Winton et al.*, 1998], a grid several orders of magnitude finer than ours. However, the grid that we use is already an order of magnitude finer than typical coupled climate models. This is not merely an artifact of our regional computational setup; a recent study diagnosing bottom water formation in ocean general circulation models finds that MITgcm, even in the ECCO global configuration, forms its deepest waters primarily through transformation of intermediate waters [*Downes et al.*, 2011]. Other models have similar and sometimes worse problems. Improved representation of bottom water formation, and its role in ocean ventilation changes under future and past climate scenarios, will require very high resolution grids or improvements to sub-grid-scale parameterizations.

[25] The melt rate magnitude and patterns of the Filchner-Ronne and western Weddell Sea ice shelves in our control experiment compare well with estimates from modern satellite data. Recent estimates from interferometric synthetic-aperture radar (InSAR) data and flux-gate modeling give a net melt rate of the combined western ice shelves in our numerical domain of 109 $\pm$ 24.8 km^3 yr^{-1} [*Joughin and Padman*, 2003; *Rignot et al.*, 2008]. In our control experiment the combined 10-year-averaged freshwater flux of these ice shelves is 111.6 km^3 yr^{-1}. In contrast the melt rates of the eastern ice shelves in our control experiment are about an order of magnitude higher than recent data estimates; we compute an average of 1071 km^3 yr^{-1} compared to an estimate of 73 $\pm$ km^3 yr^{-1} from available data [*Rignot et al.*, 2008]. Although the control melt rates of the eastern ice shelves are likely too high, this does not have a significant direct effect on the continental shelf properties and property changes in our experiments, as discussed later. Most of this meltwater is exported as buoyant surface water. However, the anomalously high meltwater flux to the surface ocean could have a damping effect on the sea ice response in our experiments. In the control, the overproduction of ice shelf meltwater could insulate the sea ice from the underlying ocean conditions. The ocean cooling in our experiments causes and thus coincides with the removal of this anomalous ice shelf freshwater, such that the sensitivity of the sea ice model in this region to changes in ocean conditions might be underestimated.

2.5. Experiments

[26] Eight numerical cooling experiments are done by changing the ocean open boundary temperatures only. The experimental boundary conditions in potential temperature, Θ_e, are defined as

$$\Theta_e = \Theta_c - \eta(\Theta_c - \Theta_{fr}) \quad (5)$$

where Θ_c is the boundary potential temperature of the control integration, Θ_{fr} is the salinity and pressure-dependent freezing point, and η ranges from 0.1 to 0.8. Thus η = 0.1 corresponds to the least cooling, while η = 0.8 represents the experiment with the most cooling. Note that each boundary grid cell can take on a different value; the boundary conditions are not homogeneous.

[27] Modification of the boundary temperatures alters the density of the boundary points with respect to those of the control. To ensure that our experiments are examining the effect of thermodynamic rather than dynamic changes, we also perform a separate set of eight "density-compensated" integrations. In addition to the temperature changes described above, in the density-compensated integrations we change the salinity of the boundary conditions; to retain the control densities with colder temperatures requires decreasing the salinity of each point. We use a local linear approximation of $\frac{\partial \rho}{\partial S}$ at each point to compute the change in salinity necessary to restore the density of the point to that of the control. The density compensated integrations result in ice melt patterns and magnitudes virtually indistinguishable from those of the non-compensated experiments, however they display a very large freshening flux from the boundaries that confuses the interpretation of our results. For this reason we discuss only the non-compensated experiments.

3. Results and Discussion

[28] We find large changes in the properties of water masses formed over the continental shelf in response to our cooling experiments. Modern water masses such as ISW, HSSW, and WDW/CDW are identified by their potential temperature and salinity. These identifying properties are exactly the properties that change with each cooling experiment. For this reason, instead of using Θ_0/S cutoff values to define water masses, we examine how properties change in fixed locations of interest. The locations which would tell us the most about modification of AABW properties would be the bottom of the Weddell Sea and the deep levels of the ocean near the northwestern edge of the Weddell Sea. However, the lack of a properly resolved or parameterized bottom boundary layer in the model restricts us to examining experimental results on and near the continental shelf.

[29] With these considerations in mind, our essential result is illustrated in Figure 4, which shows the Θ_0/S properties of water for the control and for two representative cooling sensitivity experiments at their annual salinity maxima, the time at which we expect the largest quantity of HSSW. In order to highlight changes in water masses over the continental shelf that can lead to significant changes in bottom water formation, we plot water properties of the two bottom-most layers of the domain down to the 1700-m depth cutoff and water properties inside the ice shelf cavities. Together these two layers represent, on average, $\sim$150 m of vertical

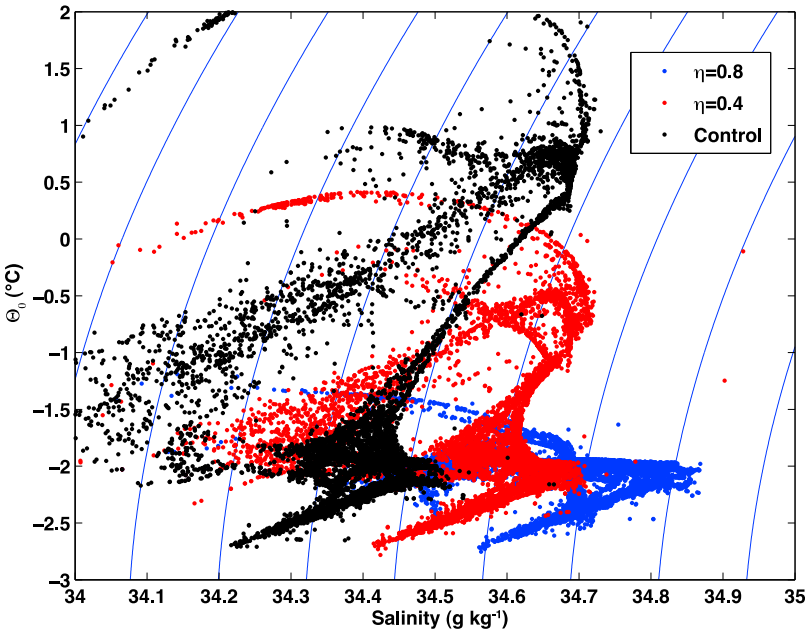

Figure 4. Θ_0/S properties of water in two layers along domain bottom down to 1700 m from the control and from two sensitivity experiments at their annual salinity maxima. Together these two layers represent, on average, ~150 m of vertical thickness. The open ocean and the shelf region west of the Antarctic Peninsula are excluded. All potential temperatures are referenced to the surface. Curved lines are isopycnals. The distance between the isopycnal lines is 0.1 kg m^{-3}.

thickness. Below ~1700 m the water properties of the control experiment are dominated by the boundary conditions. The signal of continental shelf processes, a combination of Θ_0 and S, deepens by almost 1000 m in our sensitivity experiments as the domain produces denser water able to descend farther down the continental slope; however, comparison across experiments requires a fixed-depth cutoff. The potential temperature of water in the ice shelf cavities (ISW) is already closely constrained by the in situ freezing point in the control experiment and does not change noticeably in the experiments. Water masses that correspond to modern ISW and HSSW increase significantly in salinity, up to a maximum of about 0.3 units in response to the maximum cooling experiment. At the surface freezing point, which is the temperature of HSSW, this change in salinity corresponds to an increase in surface density of 0.24 kg/m^3. This increase in surface density is equal to the modern surface density contrast between HSSW and WDW.

[30] Plotting down to the 1700-m depth encompasses the water that lies along the base of continental shelf and somewhat below the shelf break. This enables us to examine the density contrast of shelf water with the water it entrains as it descends the slope and how the contrast changes with cooler temperature experiments. There is a slight increase in salinity in the warmer, deeper water masses, but the increase is small relative to that of shelf waters. For this reason, the increase in density on the shelf in our experiments is almost identical to a change in surface density contrast between HSSW and WDW. As the continental shelf water overflows the shelf, its density contrast with the surroundings would tend to increase due to the thermobaric effect [*Killworth*, 1977]. Even without thermobaric considerations, a surface density increase of 0.24 kg/m^3 is more than double the modern density difference between NADW and AABW of about 0.1 kg/m^3.

[31] However, the density contrast between the overflow and the overlying water would also tend to decrease due to entrainment. In the modern Weddell Sea, the effect of entrainment on density contrast is small due to the weak density stratification of the water column. An increase in water column stratification, particularly if there is a large density gradient at the shelf break, can counteract the increase in overflow source density and reduce the ability of a high salinity signal to migrate from the continental shelf to the abyssal ocean [*Price and O'Neil-Baringer*, 1994]. Even if the density (and salinity) at the shelf break is increased, it does not guarantee an increase in bottom water density.

3.1. Diagnosis of Water Mass Changes: Net Salinity Fluxes and Changes

[32] Figure 5 demonstrates that the relationship between domain-averaged S and domain-averaged Θ_0 is linear, with a slope of -0.006 g kg^{-1}/°C and a maximum decrease of 0.016 g kg^{-1}. This maximum is an order of magnitude smaller than the changes in HSSW implied by Figure 4. This is because Figure 4 does not include properties of the deep or surface ocean, nor does it account for the *volume* associated with each water property pair. Salinity changes in our experiments are concentrated in particular regions of the domain.

[33] To identify the mechanisms that contribute the most to our experimental results, we consider salinity fluxes to the domain from distinct sources. While in the real ocean many of these salinity fluxes are freshwater fluxes (evaporation, precipitation, and melting), we use a volume conserving configuration of MITgcm. In this light, it is more sensible to

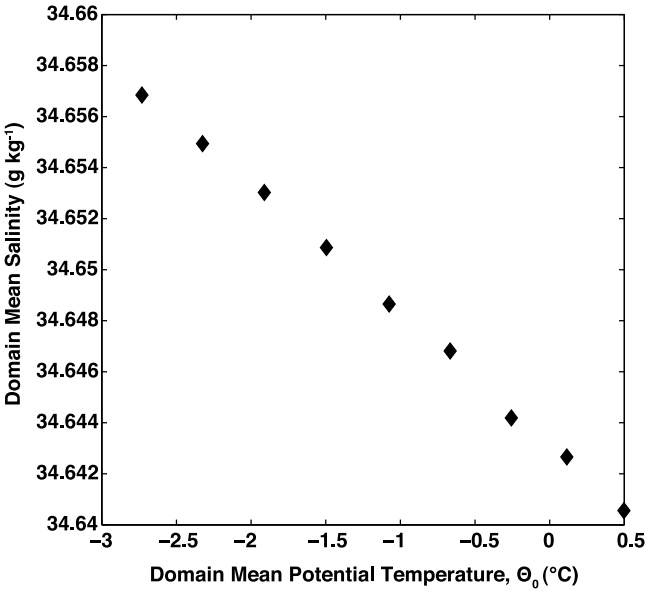

Figure 5. Sensitivity of volume-averaged domain salinity to volume-averaged domain potential temperature. All values are 10-year averages. Each experiment is represented by one point. The control experiment is at $\Theta_0 = 0.5$.

discuss salinity fluxes, keeping in mind that they have the opposite sign to freshwater fluxes.

[34] For reference, Figure 6 shows the absolute values of the salinity fluxes that contribute to the salinity of the whole domain. The bulk of our discussion will demonstrate the importance of changes in ice shelf fluxes over that of changes in sea ice fluxes across the experiments. However, it is important to keep in mind that the average salinity of water in each experiment is determined primarily by the salinity of water entering and exiting the domain and by the sea ice and surface fluxes. In the modern Weddell Sea, for example, water masses such as HSSW are higher in salinity than NADW/CDW because of sea ice formation and export. The control experiment ice shelf contribution is about an order of magnitude smaller than the sum of the other terms (Figure 6). In contrast, *changes* in the ice shelf salinity flux are an order of magnitude larger than changes in the large salt fluxes.

[35] Figure 7 is the change in salinity flux in the sensitivity experiment with respect to that of the control. Salinity is able to change in our experiments as a result of changes in evaporation, ice melting, ice freezing, and fluxes at the boundaries. Precipitation and runoff (not shown) are prescribed and do not change throughout the experiments. At first glance it seems that changes in multiple processes contribute equal magnitudes to the total salinity flux change. However, several of these processes are not independent and have a negligible combined effect.

[36] Evaporation and sea ice changes have opposite sign but are of roughly equal magnitude; that is, evaporation decreases with cooling but sea ice brine rejection and freshwater export both increase with cooling. When we calculate the evaporative flux normalized by open ocean area (not shown), we find that it is a constant for all experiments. Therefore the decrease in evaporation is primarily due to increasing sea ice cover; water under the ice can not evaporate. The sum of evaporation and sea ice changes, shown as triangles in Figure 7, contributes an order of magnitude smaller change to the domain changes in salinity than those due to changes in ice shelf and boundary fluxes.

[37] Salinity fluxes from the boundaries are due to the experimental setup. The water in the experimental domain becomes increasingly saltier with each experiment, but the velocities at the boundaries are prescribed. This leads to an increased flux of salt out of the domain of the same order of magnitude as the increase in salt flux to the domain from reduced net melting of the ice shelves, the primary source of experimental salinity flux changes. In the global ocean the exported salt would either recirculate into the Weddell Sea or be deposited at another location. The salinity stratification of both the Weddell Sea and the global ocean depends on the destination of this salt. However, because our integrations are done in a regional domain and our domain boundaries are non-interactive, the effect of this large quantity of salt is completely unknown and appears to us as a loss of salt.

[38] The ice shelf changes in melting and freezing, which have a salinifying effect on the domain as it is cooled, are an order of magnitude larger than the combined changes in surface processes, which are co-dependent. The increased boundary flux of salinity depends on the increase in domain salinity, so it is a result of the ice-shelf-induced salinity increase rather than a competing process.

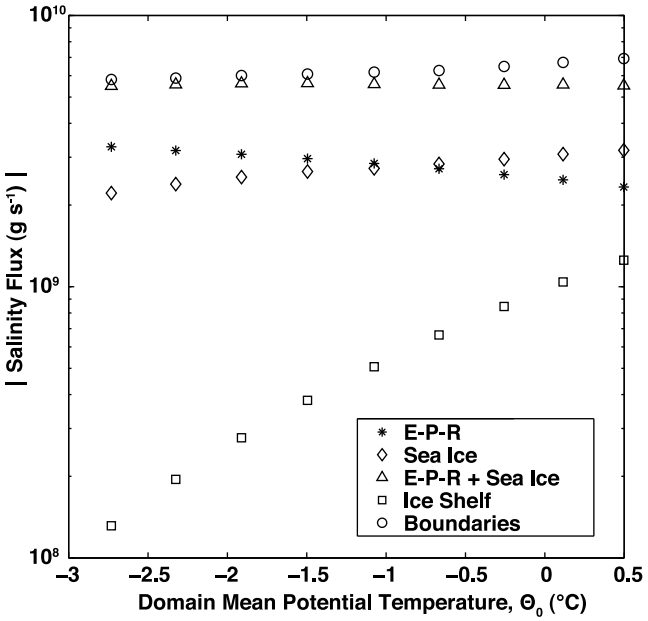

Figure 6. Magnitude of salinity fluxes integrated over the entire domain. E–P–R = evaporation - precipitation - runoff. For reference, 10^{10} g s^{-1} = 6.5 m yr^{-1} of sea ice exported (assuming a spatial cover of the total domain ocean area), so the variation between the sea ice export between the control and the coldest sensitivity experiment is ~0.82–1.03 m yr^{-1}. Precipitation and runoff are prescribed in our experiments, so the change in E–P–R is due to a change in evaporation only. The magnitude of the sea ice and evaporation contributions to domain salinity are 0.5–1 order larger than the magnitude of the ice shelf contribution in all experiments. However, the sea ice is much less sensitive to ocean temperature change than the ice shelves.

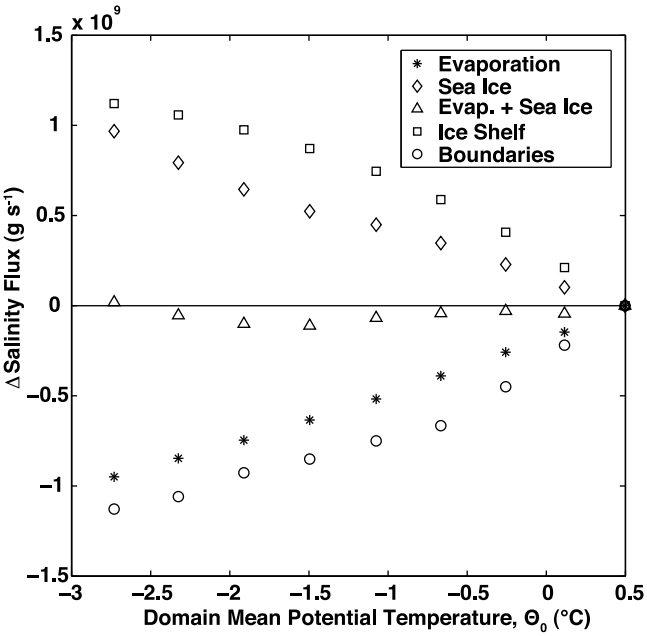

Figure 7. Change in salinity fluxes integrated over the entire domain. Each experiment is represented by the domain steady state volume-averaged potential temperature. All values are 10-year averages. For reference, 10^9 g s^{-1} = 0.65 m yr^{-1} of sea ice exported (assuming a spatial cover of the total domain ocean area). Sea ice and evaporation are of approximately equal magnitude but opposite sign. Their combination is an order of magnitude smaller than all other fluxes, that is, they essentially cancel each other's contribution.

3.2. Diagnosis of Water Mass Changes: Regional Variations and Salinity Flux Tracers

[39] There is significant spatial variation in the salinity fluxes that contribute to the domain means. Salinity fluxes due to ice shelf melting and freeze-on occur only where there are ice shelves. Perhaps less obvious is the non-uniformity in sea ice and evaporative fluxes. While in the domain average the temperature-induced increase in sea ice is balanced by a decrease in evaporation, this is not true everywhere. Figure 8 shows that in our sensitivity experiments, changes due to sea ice dominate the changes in surface salinity flux over the continental shelf. This is because in all of our experiments, and in the modern ocean, the continental shelf is almost completely covered with sea ice year-round. In our experiments there is a small increase in sea ice cover over the continental shelf, as shown in Figures 9a and 9b, which leads to a small decrease in evaporation with increasingly cool ocean temperatures. However, the increase in area and thickness of sea ice formed over the continental shelf contributes a more significant quantity of salt. In total, the change in sea ice over the continental shelf is quite small relative to the domain change, as can be seen by comparing the y-axes of Figures 7 and 8. We have not investigated the cause of the constant sea ice flux in the warmest three experiments, but one possibility is that it results from slight differences in the lateral path of the deep Weddell Gyre, which we observe in the experiments. It might also be related to the meltwater overproduction of the eastern ice shelves in the control experiment discussed previously. While the change in sea ice is important relative to other surface salinity fluxes over the continental shelf, it is small when compared to the ice shelf flux changes. Also, a change in salinity flux over the continental shelf is not equivalent to a change in continental shelf salinity.

[40] Regional variations in salinity fluxes and their distribution result in a pattern of salinity change quite different than that implied by the domain mean. With the salinity tracers described in section 2.2, we are able to determine how different processes contribute to changes in properties across experiments and where changes are concentrated geographically. To review, we have one salinity tracer that tracks salinity fluxes from the ice shelves and a second tracer that tracks the salinity fluxes from the surface. The latter is a combination of atmospheric fluxes and sea ice fluxes. However, since we showed in section 3.1 that the changes in atmospheric fluxes are due to the sea ice, it is appropriate to think of our surface tracer as equivalent to a sea ice tracer. For these analyses we define the continental shelf as the region between the ice shelf front and the 1000-m depth contour. We use 1000 m rather than 500 m in order to include water inside the Filchner and Ronne depressions on the continental shelf.

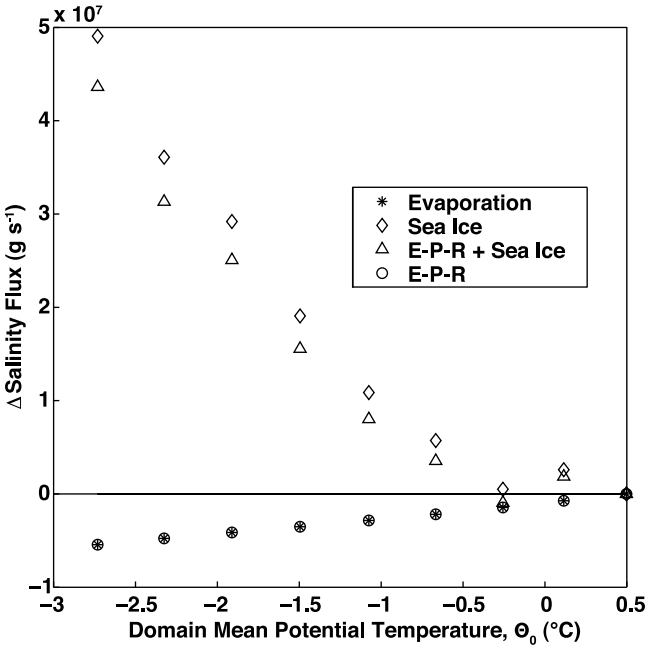

Figure 8. Change in surface salinity fluxes over the continental shelf, computed as sensitivity minus control experiment. Each experiment is represented on the x-axis by the domain steady state volume average potential temperature. All values are 10-year averages. The boundaries of the continental shelf are taken as the 1000-meter depth contour, excluding land to the north and/or west of the Antarctic Peninsula. For reference, 10^{-7} g s^{-1} is equivalent to the export of 0.11 m yr^{-1} of sea ice from the entire continental shelf. E–P–R = evaporation − precipitation − runoff. The only change in E–P–R across the experiments is due to evaporation. Salinity flux changes due to sea ice dominate the change in surface fluxes over the continental shelf.

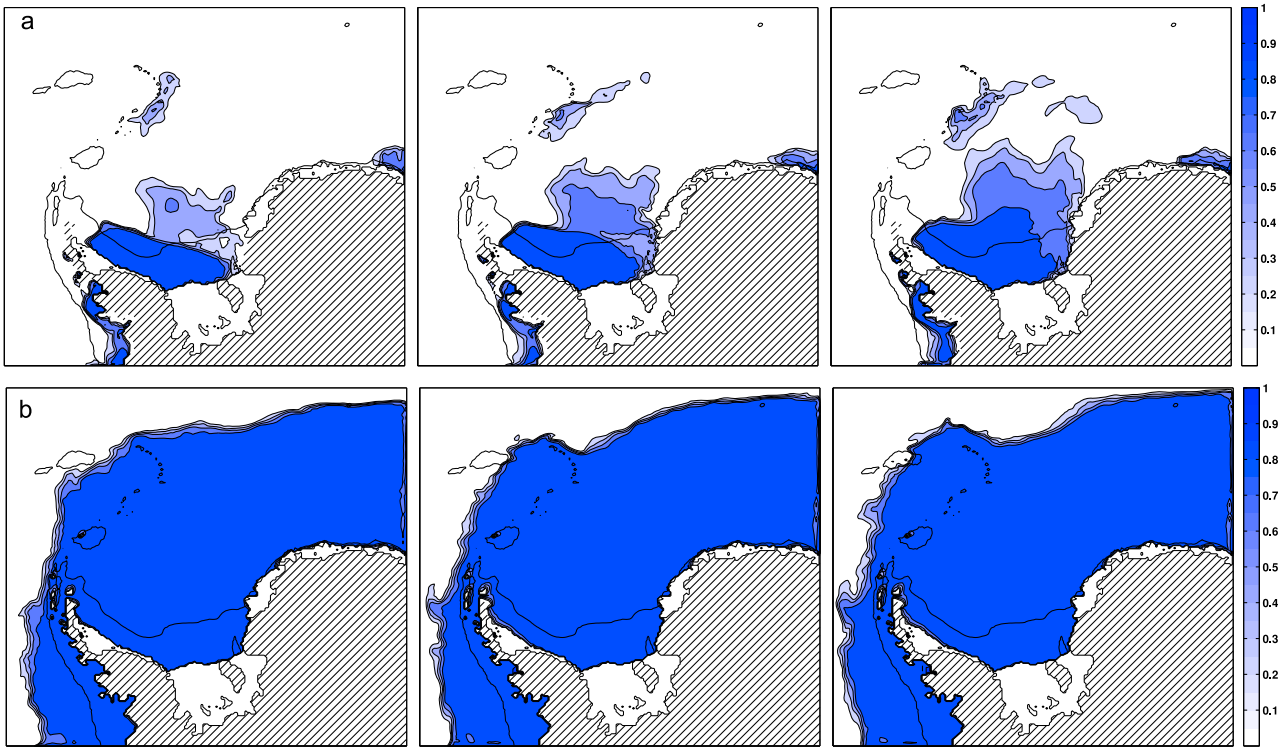

Figure 9. (a) Minimum sea ice area for three experiments, from left to right: $\eta = 0$, $\eta = 0.4$, $\eta = 0.8$. All values represent a 10-year average and a weekly average during the week in which the total sea ice volume is at its yearly minimum. (b) Maximum sea ice area for three experiments, from left to right: $\eta = 0$, $\eta = 0.4$, $\eta = 0.8$. All values represent a 10-year average and a weekly average during the week in which the total sea ice volume is at its yearly maximum. The color scale indicates grid cell concentration and is unitless. The 1000-m depth contour is overlain to indicate the continental shelf break. Grounded ice is indicated by hash marks and floating ice shelves are adjoined to the grounded ice and colored white.

[41] We find that the majority of the salinity change on the continental shelf is due to a reduction in ice shelf melting, as shown in Figures 10 and 11. The total salt flux over the continental shelf in our experiments is dominated by the sea ice, as observed today, but the change in salt flux across experiments is dominated by changes in ice sheet basal melting. Figure 10 shows the change in distribution of the surface and ice shelf tracers as vertical integrals for a representative (η = 0.4) experiment. Overall, the maximum change is largest in the ice shelf salinity tracer.

[42] The effect of the ice shelf melt changes are not only larger but also concentrated on the continental shelf. Figure 10 demonstrates that most of the change in ice shelf tracer in our experiments occurs over the continental shelf and near the shelf break, with a particularly high concentration of change inside and in the outflow from the Filchner Depression.

[43] If we consider water lying along the bottom of the continental shelf instead of the vertical integral, we find that the salinity change of bottom water precursors is predominantly due to a net reduction in ice shelf melting. Figure 11 is the evolution of salinity tracers on the bottom of the continental shelf with decreasing temperature numerical experiments. The bottom is the partially or fully water-filled grid cell above a completely land-filled cell. The computation of salinity changes in Figure 11 accounts for grid-cell volume, unlike the salinity change implied by Figure 4. We do not consider water inside ice shelf cavities, as typically this water is significantly modified by the time it reaches the shelf break. After applying these filters, the water we consider is a layer on average 67 m thick. For reference, typical observed overflow plume thicknesses in Antarctica can be anywhere from 30 to 200 m [*Muench et al.*, 2009]. In Θ_0/S space, this continental shelf water roughly corresponds to the high salinity water lying along the surface freezing line shown in Figure 4—analogous to modern ISW and HSSW. The 0.3 g kg^{-1} change in salinity as suggested by Figure 4 might not have represented a large volume of water, but when volume is accounted for, the bottom water increase in salinity is still 0.3 g kg^{-1}. Together Figures 10 and 11 demonstrate that, in our experiments, cooling continental shelf source waters increases the salinity of bottom water precursors, and this is primarily due to reduced net ice shelf basal melting.

[44] In contrast, the majority of the changes in the sea ice tracer occur away from the continental shelf and are due to an increase in average sea ice area and thickness in this region. Sea ice changes dominate the changes in salinity north of the shelf break. This increased sea ice cover north of the continental shelf break salinifies the water that would be entrained into the continental shelf overflow on its path to the bottom of the sea, although model issues prevent us from

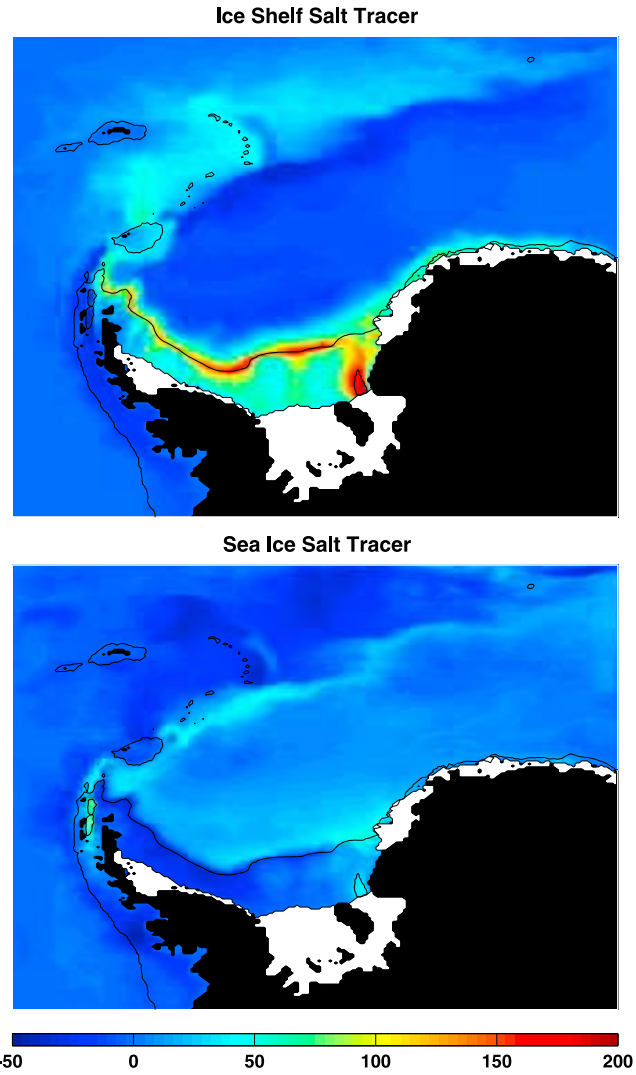

Figure 10. Depth integrated salt tracer fields for the sensitivity experiment in which the boundaries are cooled 40% toward the freezing point from the control experiment ($\eta = 0.4$). Color values are in m g kg^{-1} and represent the difference between the sensitivity and control experiments. All are 10-year averages. Black shaded area is land, white shaded area is ice shelves and the black contour line represents the location of the 1000-m bottom depth contour.

seeing how this evolves. This would reduce the density contrast between continental shelf water masses and open ocean water, and would mitigate the freshening effect of entrainment. That is, an increase in salinity off the shelf would help retain the high salinity signature of the shelf water masses throughout the shelf overflow's transformation to bottom water. In the control integration (and modern ocean) the continental shelf is perennially covered in sea ice, so the surface ocean is already at the freezing point. Under these conditions, decreasing the ocean temperature further does not have a large effect on sea ice thickness.

[45] Over the continental shelf, significant changes in sea ice, and the resultant salinity modifications, would require a large decrease in atmospheric temperature or an increase in export velocity. Lower atmospheric temperature and higher wind stress would increase the bulk heat flux between ocean and atmosphere, enabling an increase in the thickness or formation rate of sea ice. Alternatively the higher wind stress could remove thicker sea ice with the same area, or could enable faster removal of sea ice from the continental shelves, either of which would increase the net freshwater export rate. Both scenarios are certainly possible at the LGM. Atmospheric temperature and export velocities of sea ice are the same for all experiments, so the primary way for ice export to increase in our experiments is through an increase in ice thickness.

3.3. Diagnosis of Water Mass Changes: Regional Differences in Ice Shelves

[46] Although the shapes and sizes of the ice shelves are fixed in our experiments, they vary across the numerical domain. The smaller, shallower, ice shelves to the east of the Filchner-Ronne Ice Shelf are more sensitive to changes in the boundary temperature forcing. Comparing the total melt rate of the large ice shelves with that of the smaller ice shelves in the east of our numerical domain (Figure 12), we find that there is a greater cumulative flux of meltwater from the small eastern shelves than from the large shelves, except in the coldest experiment. This does not mean that all of this water makes it into the Weddell Sea proper; the majority is so buoyant that it rises to the surface and is exported from the domain.

[47] The large change in freshwater flux from the eastern shelves is not the determining factor in our results. With our current tools we can not distinguish the geographical source of the ice shelf salinity forcing in our salt tracers. However, we can compute the reduction in freshwater flux from different regions required to cause the changes in salt tracers on the continental shelf. The volume of water we consider to define the continental shelf (up to the 1000-m contour) is 3.77×10^{13} m^3. Assuming a typical density of salt water of 1027.5 kg m^{-3} and that of glacial meltwater of 999.8 kg m^{-3}, a maximum change in salinity of 0.3 g kg^{-1}, and using the model salt-to-freshwater conversion factor of 33.4 g kg^{-1}, we find that a net 3.48×10^{11} m^3 of meltwater is required to explain the maximum difference in salinity between the control and the coldest experiment. If the residence time of these waters on the shelf is one year, that corresponds to a difference in freshwater input of 3.48×10^{11} m^3 yr^{-1}. If instead the continental shelf water is completely renewed only every 10 years, the difference in freshwater flux required to maintain this salinity difference between the two experiments is an order of magnitude smaller. The maximum difference in freshwater flux magnitude from the western ice shelves is only 2.83×10^{10} m^3 yr^{-1}, which means that unless the residence time of water on the shelf is more than 10 years, some change in freshwater flux from the eastern ice shelves is necessary to explain the observed changes in our experiments. This is expected, because our definition of the continental shelf includes the shelf directly in front of the eastern ice shelves. The combined shelf area in front of the eastern ice shelves is only 1/3 of the continental shelf area lying inside the Weddell Sea, so for the eastern shelf change to impose a bias on our average result, there would need to be an excessive change in salinity. However, our average continental shelf answer is not biased by a large change over the eastern continental shelves. Rather the maximum (coldest

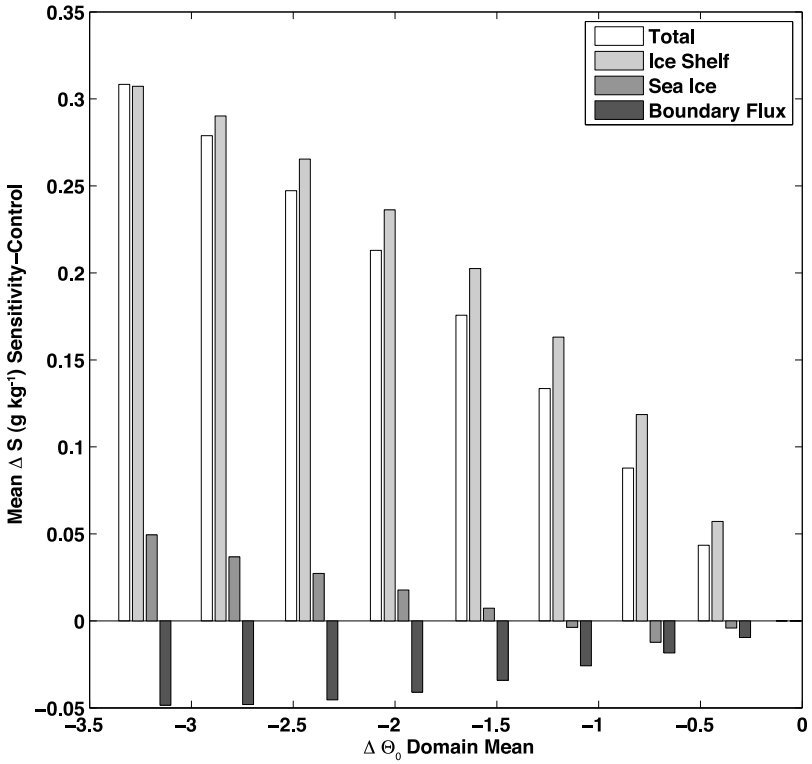

Figure 11. Ice shelf and sea ice salinity tracer values integrated over the bottom water-filled layer on the continental shelf. All values represent the 10-year-averaged difference between sensitivity and control. The boundaries of the continental shelf are taken as the area between the ice shelf front and the 1000-m depth contour, shown in Figure 2, excluding land to the north and/or west of the Antarctic Peninsula.

experiment) average change in ice shelf salinity tracer over the continental shelf abutting the eastern ice shelves is only 0.25 g/kg, whereas over the main continental shelf in the Weddell Sea proper, the change is 0.33 g/kg.

[48] Hypothetically, if a reduction in eastern melt rates was large enough, the increase in salinity, besides affecting western shelf processes, could also enable direct bottom water formation from the eastern continental shelves. Today, water formed through interactions with the eastern ice shelves does find its way onto the continental shelves in the Weddell Sea. By preconditioning the water properties that enter the Weddell Sea, the eastern shelf interactions indirectly affect the bottom water formation processes to the west, although the relative magnitude of the eastern shelf contribution is still uncertain [*Nicholls et al.*, 2009]. However, the extremely low salinity in front of the eastern ice shelves suppresses direct bottom water formation [*Fahrbach et al.*, 1994].

3.4. Relevance to Glacial Oceans

[49] We do not simulate the LGM. As such, it is difficult to compare our sensitivity experiments to data, because we purposely do not modify a large number of important variables. However, we believe that the sensitivity experiment that is most appropriate to compare to LGM data is our most extreme temperature scenario. First, the temperature changes of interest to the LGM ocean are not as large as the domain-averaged temperature suggests. The temperature change on the shelf is much smaller than the average temperature change of the whole domain, which is significant because a large volume of deep water in our domain does not interact with the continental shelf. Using the same definition of continental shelf as for the salinity tracers, we find that the average potential temperature on the continental shelf in our most extreme experiment is −2.00°C. In comparison, the average potential temperature on the continental shelf in our control is −1.65°C. The sensitivity of continental shelf salinity to continental shelf temperature is thus much higher than the sensitivity of the whole domain salinity to whole domain temperature: 0.857 g kg^{-1}/°C as opposed to 0.006 g kg^{-1}/°C. Given these considerations, a 0.3 g kg^{-1} change in salinity due to a continental shelf potential temperature decrease of 0.35°C is reasonable. It does not require unphysically cold temperatures. With a simple change in temperature we can account for 30% of the difference in salinity contrast observed between GNAIW and GSSBW.

[50] We do not address how the temperature at the boundaries of our computational Weddell Sea domain could be depressed to such low levels. There are two possibilities: (i) either the temperature of WDW/CDW was lower or (ii) relatively warm CDW did not intrude onto the continental shelves. Our setup does not favor one or the other of these hypotheses—we simply make the water colder. So, even if northern source deep water was not a precursor to GSSBW at the LGM, the fact that the ocean was cooler still

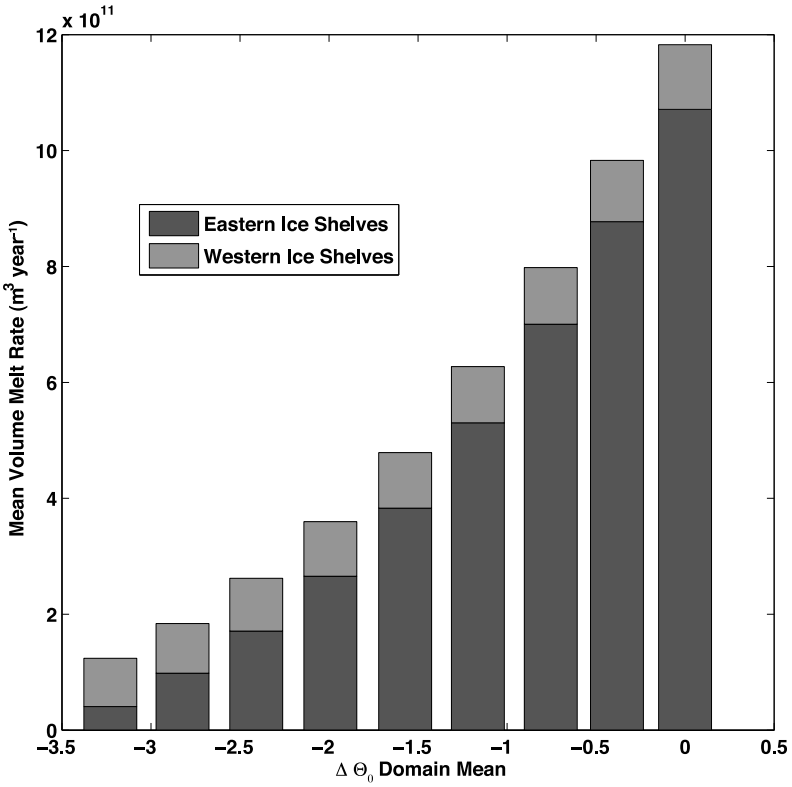

Figure 12. Comparison of time-averaged and spatially-integrated volume melt rate of ice shelves in western and eastern sectors of domain. The western sector corresponds to the Filchner-Ronne Ice Shelf and all ice shelves in the Western Weddell Sea. The eastern sector is all ice shelves to the east of the Filchner-Ronne Ice Shelf. All values represent the 10-year-average of a spatial integration.

explains a significant fraction of the high measured bottom water salinity.

3.5. The Effect of Unmodeled Processes

[51] In order to focus on the sensitivity of bottom water formation to ocean temperature, we do not simulate the LGM. As previously discussed, a change in wind stress and/or atmospheric temperature could have an important role in changing the bottom water properties. In addition, there is evidence that both atmospheric temperature over Antarctica [*Petit et al.*, 1999] and sea surface temperature in the Southern Ocean [*Gersonde et al.*, 2005] were lower at the LGM than they are today. All of these factors could contribute to increasing the sea ice export. Increased sea ice export from LGM deep water formation sites probably played a larger role in increasing the salinity of LGM bottom water than it does in our experiments, but we specifically do not simulate that.

[52] Another factor that we do not consider is a change in bathymetry of the land or ice shelf cavities. However, in our experiments the smaller ice shelves showed the greatest change in melt rate in the experiments. Isolated ice shelf cavity process studies also indicate that ice shelf basal melting depends strongly on ice sheet morphology [*Little et al.*, 2009]. This is significant to inferred ice shelf conditions at the LGM. Reconstructions of the LGM Antarctic ice sheet extent suggest that the grounding line was located further north [*Anderson et al.*, 2002], which could mean that the ice shelves at the LGM were configured similarly to the small ice shelves located to the east of the Weddell Sea in our experiments: either shallow and abutted by a narrow continental shelf or overhanging the continental shelf break. The fact that melt rates of these smaller ice shelves are more sensitive to temperature could mean that temperature played a greater relative role in setting shelf water salinity than it does with the modern shelf configuration that we used in our experiments. In short, given the correct ice sheet and ice shelf shapes at the LGM, small perturbations in temperature might generate a larger ice shelf salinity response.

[53] It is important to remember that the ice sheet morphology dynamically responds to changes in ocean conditions, a factor we have neglected by using fixed-shape ice shelf cavities. The inclusion of tides, which are influenced by ice shelf cavity and continental shelf shapes, could change the total Filchner-Ronne ice shelf melt rate by an order of magnitude [*Makinson et al.*, 2011]. It is also possible that the outward migration of the ice sheet grounding line meant that there was no Antarctic continental shelf or ice shelves, in which case the bottom water formation process at the LGM would have been fundamentally different [*Paillard and Parrenin*, 2004].

[54] Besides water properties, bottom water formation depends heavily on the rate of production and movement off the shelf. The modern production rate suggests that the residence time of high density water on the continental shelf is between 5 and 7 years [*Gill*, 1973; *Gordon et al.*, 2010].

While water does leave our domain, the open boundary configuration fixes its export rate.

4. Conclusions

[55] Cooling the ocean has a significant effect on the salinity of the water lying on the continental shelf of the Weddell Sea, water that in the modern is a precursor to Antarctic Bottom Water. Pore fluid measurements find that the salinity gradient between GSSBW and GNAIW was 1.1 units greater than the gradient between AABW and NADW. With ocean cooling alone, we can explain as much as 30% of this difference in salinity stratification. Almost all of this change is due to a reduction of basal melting from marine-based ice sheets over and in the vicinity of the Weddell Sea continental shelf, but a small portion can also be attributed to the export of thicker sea ice. Similar changes in ice shelf basal melting could have occurred over the other Antarctic continental shelves at the LGM, which in addition to transport and recirculation of circumpolar water masses, might have increased the contribution of this particular effect. The effect we observe in our experiments is due primarily to thermodynamics and not to a dynamic (i.e., buoyancy-driven) response to temperature changes; while ocean temperature can not account for all of the measured salinity difference between GSSBW and AABW, it is of the same order of magnitude and must be considered as one of several important salinity drivers.

[56] While this is a significant number, it can not explain all of the change in salinity. Among the candidates for explaining the remaining 70%, ice shelf shape and wind-driven changes in sea ice processes are likely to have significant roles. Bathymetric changes at the LGM, including the shape and exposure of the continental shelf and ice shelves, as well as their effect on tidal mixing, may have been important in setting the salinity of GSSBW. In our experiments, small ice shelves, such as those that may have existed at the LGM, were more sensitive to changes in ocean temperature than the larger ones, perhaps due to their greater exposure to open ocean conditions. In the modern ocean, this sensitivity and exposure to warm ocean conditions contribute to blocking direct bottom water formation in front of the small ice shelves, such that processes over smaller continental shelves, in front of smaller ice shelves, have only an indirect role in bottom water formation. In a reduced open ocean temperature environment this constraint might have been lifted, such that significant bottom water formation could have occurred in front of small ice shelves. With a narrow and more spatially homogeneous continental shelf ringing the Antarctic continent, bottom water formation may have been more geographically distributed than it is today. Decreased atmospheric temperature and increased wind stress near the Antarctic continent also may have contributed to an increased salinity flux from sea ice formation and export. Our experiments show that a decrease in ocean temperature alone does not significantly increase the ocean salinification due to sea ice export, in part because greater sea ice cover reduces ocean evaporation. Due to the limitations of a regional model in representing water export rates, future studies on this subject should investigate the feedback between changes in property (Θ_0, S) and density stratification in a circumpolar or global configuration.

[57] **Acknowledgments.** M.D.M. and J.F.A. received funding from the National Science Foundation under NSF grant OCE-0929272. M.D.M., D.M., and M.P.S. received funding from the ECCO2 project, a contribution to the NASA Modeling Analysis and Prediction (MAP) Program. We gratefully acknowledge computational resources and support from the NASA Advanced Supercomputing (NAS) Division. We thank Keith Nicholls for providing the data for Figure 1. Anand Gnanadesikan inspired writing the salt tracer code for analyzing the sources of salinity changes. We are grateful to Martin Losch for his implementation of the ice shelf code in MITgcm and for helpful discussions about ice shelf and sea ice modeling.

References

Adcroft, A., C. Hill, and J. Marshall (1997), The representation of topography by shaved cells in a height coordinate model, *Mon. Weather Rev.*, *125*(9), 2293–2315.

Adkins, J., K. McIntyre, and D. Schrag (2002), The salinity, temperature and $\delta^{18}O$ of the glacial deep ocean, *Science*, *298*(5599), 1769–1773.

Adler, R. F., et al. (2003), The version-2 global precipitation climatology project (gpcp) monthly precipitation analysis (1979–present), *J. Hydrometeorol.*, *4*, 1147–1167.

Anderson, J. B., S. Shipp, A. Lowe, J. Wellner, and A. Mosola (2002), The Antarctic Ice Sheet during the Last Glacial Maximum and its subsequent retreat history: A review, *Quat. Sci. Rev.*, *21*, 49–70.

Antonov, J. I., et al. (2010), *World Ocean Atlas 2009*, vol. 2, *Salinity*, *NOAA Atlas NESDIS*, vol. 69, edited by S. Levitus, 184 pp., NOAA, Silver Spring, Md.

Bouttes, N., D. Roche, and D. Paillard (2009), Impact of strong deep ocean stratification on the glacial carbon cycle, *Paleoceanography*, *24*, PA3203, doi:10.1029/2008PA001707.

Bouttes, N., D. Paillard, and D. Roche (2010), Impact of brine-induced stratification on the glacial carbon cycle, *Clim. Past*, *6*(5), 575–589.

Chappell, J., and N. Shackleton (1986), Oxygen isotopes and sea level, *Nature*, *324*(13), 137–140.

Cutler, K., et al. (2003), Rapid sea-level fall and deep-ocean temperature change since the last interglacial period, *Earth Planet. Res. Lett.*, *206*, 253–271.

DiMarzio, J., A. Brenner, R. Schutz, C. Shuman, and H. Zwally (2007), GLAS/ICESat 500 m laser altimetry digital elevation model of Antarctica, http://nsidc.org/data/nsidc-0304.html, Natl. Snow and Ice Data Cent. Boulder, Colo.

Downes, S. M., A. Gnanadesikan, S. M. Griffies, and J. L. Sarmiento (2011), Water mass exchange in the Southern Ocean in coupled climate models, *J. Phys. Oceanogr.*, *41*, 1756–1771, doi:10.1175/2011JPO4586.1.

Fahrbach, E., R. Peterson, G. Rohardt, P. Schlosser, and R. Bayer (1994), Supression of bottom water formation in the southeastern Weddell Sea, *Deep Sea Res., Part I*, *41*(2), 389–411.

Fahrbach, E., G. Rohardt, N. Scheele, M. Schröder, V. Strass, and A. Wisotzki (1995), Formation and discharge of deep and bottom water in the northwestern Weddell Sea, *J. Mar. Res.*, *53*(4), 515–538.

Foldvik, A., T. Gammelsrød, S. Østerhus, E. Fahrbach, G. Rohardt, M. Schröder, K. W. Nicholls, L. Padman, and R. A. Woodgate (2004), Ice shelf water overflow and bottom water formation in the southern Weddell Sea, *J. Geophys. Res.*, *109*, C02015, doi:10.1029/2003JC002008.

Gent, P. R., and J. C. McWilliams (1990), Isopycnal mixing in ocean circulation models, *J. Phys. Oceanogr.*, *20*, 150–155.

Gersonde, R., X. Crosta, A. Abelmann, and L. Armand (2005), Sea-surface temperature and sea ice distribution of the Southern Ocean at the EPILOG Last Glacial Maximum—A circum-Antarctic view based on siliceous microfossil records, *Quat. Sci. Rev.*, *24*, 869–896.

Gill, A. (1973), Circulation and bottom water production in the Weddell Sea, *Deep Sea Res. Oceanogr. Abstr.*, *20*(2), 111–140.

Gordon, A., B. Huber, D. McKee, and M. Visbeck (2010), A seasonal cycle in the export of bottom water from the Weddell Sea, *Nat. Geosci.*, *3*(8), 551–556.

Griffies, S. (1998), The Gent-McWilliams skew flux, *J. Phys. Oceanogr.*, *28*(5), 831–841.

Hall, B. (2009), Holocene glacial history of Antarctica and the sub-Antarctic islands, *Quat. Sci. Rev.*, *28*, 2213–2230.

Harms, S., E. Fahrbach, and V. Strass (2001), Sea ice transports in the Weddell Sea, *J. Geophys. Res.*, *106*(C5), 9057–9073.

Hellmer, H. (2004), Impact of Antarctic ice shelf basal melting on sea ice and deep ocean properties, *Geophys. Res. Lett.*, *31*, L10307, doi:10.1029/2004GL019506.

Hellmer, H., and D. Olbers (1989), A two-dimensional model of the thermohaline circulation under an ice shelf, *Antarct. Sci.*, *1*(4), 325–336.

Holland, D., and A. Jenkins (1999), Modelling thermodynamic ice-ocean interactions at the base of an ice shelf, *J. Phys. Oceanogr.*, *29*(8), 1787–1800.

Jackett, D., T. McDougall, R. Feistel, D. Wright, and S. Griffies (2006), Algorithms for density, potential temperature, conservative temperature, and the freezing temperature of seawater, *J. Atmos. Oceanic Technol.*, *23*(12), 1709–1728.

Jenkins, A., H. Hellmer, and D. Holland (2001), The role of meltwater advection in the formulation of conservative boundary conditions at an ice-ocean interface, *J. Phys. Oceanogr.*, *31*(1), 285–296.

Joughin, I., and L. Padman (2003), Melting and freezing beneath Filchner-Ronne Ice Shelf, Antarctica, *Geophys. Res. Lett.*, *30*(9), 1477, doi:10.1029/2003GL016941.

Killworth, P. (1977), Mixing on the Weddell Sea continental slope, *Deep Sea Res.*, *24*, 427–448.

Kwok, R., A. Schweiger, D. Rothrock, S. Pang, and C. Kottmeier (1998), Sea ice motion from satellite passive microwave data assessed with ERS SAR and buoy data, *J. Geophys. Res.*, *103*(C4), 8191–8214.

Large, W. G., and S. Pond (1982), Sensible and latent heat flux measurements over the ocean, *J. Phys. Oceanogr.*, *12*, 464–482.

Large, W. G., and S. G. Yeager (2004), Diurnal to decadal global forcing for ocean and sea-ice models: The data sets and flux climatologies, *Tech. Note TN-460+STR*, Natl. Cent. for Atmos. Res., Boulder, Colo.

Large, W. G., J. C. McWilliams, and S. Doney (1994), Oceanic vertical mixing: A review and a model with a nonlocal boundary layer parameterization, *Rev. Geophys.*, *32*(4), 363–403.

Large, W. G., G. Danabasoglu, S. C. Doney, and J. C. McWilliams (1997), Sensitivity to surface forcing and boundary layer mixing in a global ocean model: Annual-mean climatology, *J. Phys. Oceanogr.*, *27*, 2418–2447.

Legg, S., R. W. Hallberg, and J. Girton (2006), Comparison of entrainment in overflows simulated by z-coordinate, isopycnal and non-hydrostatic models, *Ocean Modell.*, *11*(1–2), 69–97.

Little, C., A. Gnanadesikan, and M. Oppenheimer (2009), How ice shelf morphology controls basal melting, *J. Geophys. Res.*, *114*, C12007, doi:10.1029/2008JC005197.

Locarnini, R., et al. (2010), *World Ocean Atlas 2009*, vol. 1, *Temperature*, *NOAA Atlas NESDIS*, vol. 68, edited by S. Levitus, 184 pp., NOAA, Silver Spring, Md.

Losch, M. (2008), Modeling ice shelf cavities in a z coordinate ocean general circulation model, *J. Geophys. Res.*, *113*, C08043, doi:10.1029/2007JC004368.

Losch, M., D. Menemenlis, J.-M. Campin, P. Heimbach, and C. Hill (2010), On the formulation of sea-ice models. part 1: Effects of different solver implementations and parameterizations, *Ocean Modell.*, *33*(1–2), 129–144.

Lythe, M., D. Vaughan, and the BEDMAP Consortium (2001), BEDMAP: A new ice thickness and subglacial topographic model of Antarctica, *J. Geophys. Res.*, *106*(B6), 11,335–11,351.

Makinson, K., P. Holland, A. Jenkins, K. Nicholls, and D. Holland (2011), Influence of tides on melting and freezing beneath Filchner-Ronne Ice Shelf, Antarctica, *Geophys. Res. Lett.*, *38*, L06601, doi:10.1029/2010GL046462.

Malone, M., J. Martin, J. Schönfeld, U. Ninnemann, D. Nürnberg, and T. White (2004), The oxygen isotopic composition and temperature of Southern Ocean bottom waters during the Last Glacial Maximum, *Earth Planet. Res. Lett.*, *222*(1), 275–283.

Marks, K. M., and W. H. F. Smith (2006), An evaluation of publicly available global bathymetry grids, *Mar. Geophys. Res.*, *27*, 19–34.

Marshall, J., A. Adcroft, C. Hill, L. Perelman, and C. Heisey (1997a), A finite-volume, incompressible Navier-Stokes model for studies of the ocean on parallel computers, *J. Geophys. Res.*, *102*(C3), 5753–5766.

Marshall, J., C. Hill, L. Perelman, and A. Adcroft (1997b), Hydrostatic, quasi-hydrostatic and non-hydrostatic ocean modeling, *J. Geophys. Res.*, *102*(C3), 5733–5752.

Menemenlis, D., I. Fukumori, and T. Lee (2005), Using Green's functions to calibrate an ocean general circulation model, *Mon. Weather Rev.*, *133*(5), 1224–1240.

Menemenlis, D., et al. (2008), ECCO2: High resolution global ocean and sea ice data synthesis, *Mercator Ocean Q. Newsl.*, *31*, 13–21.

Muench, R., A. Wåhlin, T. Özgökmen, R. Hallberg, and L. Padman (2009), Impacts of bottom corrugations on a dense Antarctic outflow: NW Ross Sea, *Geophys. Res. Lett.*, *36*, L23607, doi:10.1029/2009GL041347.

Nguyen, A. T., D. Menemenlis, and R. Kwok (2011), Arctic ice-ocean simulation with optimized model parameters: approach and assessment, *J. Geophys. Res.*, *116*, C04025, doi:10.1029/2010JC006573.

Nicholls, K., S. Østerhus, K. Makinson, T. Gammelsrød, and E. Fahrbach (2009), Ice-ocean processes over the continental shelf of the southern Weddell Sea, *Rev. Geophys.*, *47*, RG3003, doi:10.1029/2007RG000250.

Orsi, A., G. Johnson, and J. Bullister (1999), Circulation, mixing and production of Antarctic Bottom Water, *Prog. Oceanogr.*, *43*(1), 55–109.

Paillard, D., and F. Parrenin (2004), The Antarctic ice sheet and the triggering of deglaciations, *Earth Planet. Res. Lett.*, *227*, 263–271.

Petit, J., et al. (1999), Climate and atmospheric history of the past 420,000 years from the Vostok ice core, Antarctica, *Nature*, *399*(6735), 429–436.

Price, J., and M. O'Neil-Baringer (1994), Outflow and deep water production by marginal seas, *Prog. Oceanogr.*, *33*(3), 161–200.

Redi, M. (1979), Oceanic isopycnal mixing by coordinate rotation, *J. Phys. Oceanogr.*, *12*, 1154–1158.

Reid, J., and R. Lynn (1971), On the influence of the Norwegian-Greenland and Weddell seas upon the bottom waters of the Indian and Pacific oceans, *Deep Sea Res.*, *18*, 1063–1088.

Rignot, E., J. L. Bamber, M. R. van den Broeke, C. Davis, Y. Li, W. J. van de Berg, and E. van Meijgaard (2008), Recent Antarctic ice mass loss from radar interferometry and regional climate modelling, *Nat. Geosci.*, *1*, 106–110.

Schrag, D., J. Adkins, K. McIntyre, J. Alexander, D. Hodell, C. Charles, and J. McManus (2002), The oxygen isotopic composition of seawater during the Last Glacial Maximum, *Quat. Sci. Rev.*, *21*, 331–342.

Toggweiler, J., and B. Samuels (1995), The effect of sea ice on the salinity of Antarctic bottom waters, *J. Phys. Oceanogr.*, *25*, 1980–1997.

Toggweiler, J., J. Russell, and S. Carson (2006), Midlatitude westerlies, atmospheric CO_2, and climate change during the ice ages, *Paleoceanography*, *21*, PA2005, doi:10.1029/2005PA001154.

Uppala, S. M., et al. (2005), The ERA-40 re-analysis, *Q. J. R. Meteorol. Soc.*, *131*, 2961–3012.

van den Broeke, M., W. van de Berg, and E. van Meijgaard (2008), Firn depth correction along the Antarctic grounding line, *Antarct. Sci.*, *20*, 513–517.

Whitehouse, P., M. Bentley, and A. L. Brocq (2012), A deglacial model for Antarctica: Geological constraints and glaciological modelling as a basis for a new model of Antarctic glacial isostatic adjustment, *Quat. Sci. Rev.*, *32*, 1–24.

Winton, M., R. Hallberg, and A. Gnanadesikan (1998), Simulation of density-driven frictional downslope flow in z-coordinate ocean models, *J. Phys. Oceanogr.*, *28*, 2163–2174.

Zwally, H., J. Comiso, C. Parkinson, D. Cavalieri, and P. Gloersen (2002), Variability of Antarctic sea ice 1979–1998, *J. Geophys. Res.*, *107*(C5), 3041, doi:10.1029/2000JC000733.